Chemical Identification of Interlayer Contaminants within van der Waals Heterostructures

Jeffrey J. Schwartz,[†,‡] *Hsun-Jen Chuang,*[§] *Matthew R. Rosenberger,*[§] *Saujan V. Sivaram,*[§] *Kathleen M. McCreary,*[§] *Berend T. Jonker,*[*,§] *Andrea Centrone,*[*,†]

[†]Physical Measurement Laboratory, National Institute of Standards and Technology, Gaithersburg, MD 20899, United States

[‡]Institute for Research in Electronics and Applied Physics, University of Maryland, College Park, MD 20742, United States

[§]Materials Science & Technology Division, Naval Research Laboratory, Washington, D.C. 20375, United States

KEYWORDS: van der Waals heterostructures, 2D materials, interlayer contaminants, nanoscale spectroscopy, photothermal induced resonance, IR spectroscopy

ABSTRACT:

Van der Waals heterostructures (vdWHs) leverage the characteristics of two-dimensional (2D) material building blocks to create a myriad of structures with unique and desirable properties. Several commonly employed fabrication strategies rely on polymeric stamps to assemble layers of 2D materials into vertical stacks. However, the properties of such heterostructures frequently are degraded by contaminants, typically of unknown composition, trapped between the constituent layers. Such contaminants therefore impede studies of the intrinsic properties of heterostructures and hinder their application. Here, we use the photothermal induced resonance (PTIR) technique to obtain infrared spectra and maps of the contaminants down to a few attomoles and with nanoscale resolution. Heterostructures comprised of WSe_2, WS_2, and hBN layers were found to contain significant amounts of polydimethylsiloxane (PDMS) and polycarbonate, corresponding to the stamp materials used in their construction. Additionally, we verify that an atomic force microscope-based "nano-squeegee" technique is an effective method for locally removing contaminants by comparing spectra within as-fabricated and cleaned regions. Having identified the source of the contaminants, we demonstrate that cleaning PDMS stamps with isopropanol or toluene prior to vdWH fabrication reduces PDMS contamination within the structures. The general applicability of the PTIR technique for identifying the sources corrupting vdWHs provides valuable guidance for devising mitigation strategies (e.g., stamp cleaning or pre-/post-treatments) and enhances capabilities for producing materials with precisely engineered properties.

INTRODUCTION

Two-dimensional (2D) materials are composed of layers that are weakly bound to each other via van der Waals forces. This characteristic enables facile mechanical isolation, pick up, and transfer of few or single layers from bulk crystals. The family of 2D materials includes metals such as graphene,[1] semiconductors such as the transition metal dichalcogenides (TMDs),[2] and insulators such as hexagonal boron nitride (hBN).[3] Individually, single layers of these materials attract much attention due to their diverse and exceptional electronic, optical, and magnetic properties.[4–6] Notably, the absence of out-of-plane covalent bonding enables restacking of multiple individual layers in any sequence without regard for lattice match, providing an unprecedented opportunity to create synthetic heterostructures with tailored properties.[7–9] These stacks, referred to as van der Waals heterostructures (vdWHs), can provide novel functionalities and open new opportunities in optoelectronics,[2] valleytronics,[10] and catalysis,[11] while revealing new physics.[12]

A common fabrication route for vdWHs involves the pick-up, transfer, and release of selected layers onto a target substrate. This process is already achievable with a variety of techniques: the poly-methyl methacrylate (PMMA) carrying layer,[13] the wedge transfer,[14] the polydimethylsiloxane (PDMS) deterministic all-dry transfer,[15] and the van der Waals pick-up transfer[16] methods. However, these stacking methods unintentionally trap material, typically of unknown composition, between the layers, even when carried out in nominally clean environments (e.g., glove boxes or at reduced pressures). These trapped contaminants obstruct intimate contact between the layers and often lead to the formation of numerous sub-surface aggregates, which appear as protrusions (“bubbles” or “blisters”) and other topographic irregularities in vdWHs.[17] Previously, it was reported that the bubbles observed in vdWHs constructed using the PMMA carrying layer method contained amorphous hydrocarbons, as would be expected in the case of

PMMA contamination.[18] However, little is known about the contaminants trapped by other transfer methods. These contaminants preclude the formation of pristine interfaces, modulate material properties, hinder interlayer interactions (e.g., charge and energy transfer),[19] and promote degradation of delicate 2D materials such as black phosphorus.[20,21]

Common strategies for limiting contamination and for promoting intimate layer contacts include control of the transfer and peeling speed or thermal annealing. Annealing promotes contaminant aggregation through Ostwald ripening of the bubbles and diffusion of contaminants out of the vdWHs through the edges,[22] thereby leaving behind wider, possibly pristine regions, but leads to unpredictable contaminant distributions. Recently, controllable, bubble-free regions in vdWHs were prepared either by using the tip of an atomic force microscope (AFM) probe to sweep ("squeegee") an area of interest[23,24] or by stacking the 2D materials under vacuum.[25] However, the fabrication of "clean" interfaces using typical transfer procedures remains a significant challenge that must be resolved to fully realize the potential of vdWHs in widespread applications. Consequently, novel analytical methods capable of both high chemical sensitivity and nanoscale resolution are necessary to identify the minute quantities of interlayer contaminants. Such knowledge will provide valuable guidance for devising mitigation strategies that improve the efficacies of vdWH fabrication and for producing precisely engineered nanostructures.

Here, we leverage photothermal induced resonance (PTIR),[26,27] a chemically sensitive scanning probe technique to identify the chemical compositions of nanoscale contaminants trapped within vdWHs fabricated using polymeric stamps; i.e., the most common transfer techniques. The close correspondence between PTIR and well-known far-field infrared (IR) spectra,[28–30] enables the identification of PDMS or polycarbonate (PC) contaminants, matching the stamp materials used in vdWH fabrication. As few as $\approx 10^{-18}$ mol of contaminants were detected in single

nanobubbles. We verify that using an AFM-based nano-squeegee technique is a generally effective, albeit low-throughput, method to create contaminant-free areas in vdWHs without thermal annealing. Additionally, having identified the trapped impurities and their likely sources, we find that washing PDMS stamps with isopropanol or toluene prior to pick-up is effective at reducing the amount of polymeric residue transferred by the stamp. Based on the wide applicability of PTIR,[26,27] we believe that our approach will be generally useful to engineer cleaner vdWHs and to characterize nanostructures with precisely controlled properties.

RESULTS AND DISCUSSION

Infrared micro-spectroscopy is a diffraction-limited technique widely used to identify materials and chemical impurities but lacks the sensitivity and spatial resolution to characterize the nanoscale contaminants studied here. By contrast, PTIR,[26,27] also known as AFM-IR, bypasses light diffraction limitations using a sharp AFM probe as a near-field mechanical transducer, thereby enabling IR characterization with nanoscale resolution and high sensitivity. In PTIR, a pulsed, wavelength-tunable, monochromatic laser (Figure 1b) illuminates a portion of the sample (≈ 50 μm diameter) centered around an AFM tip in contact with the sample. Within the illuminated area, the sample constituents that absorb the laser pulse undergo rapid thermal expansion and, among those areas, only the portion of the sample directly beneath the AFM probe contributes to the PTIR signal. The sample expansion dynamics can be captured directly using ultrasensitive, custom-made nanophotonic probes,[31] but this expansion is too fast for conventional AFM cantilevers, which instead are kicked into oscillations akin to a struck tuning fork. Because the cantilever oscillation amplitude is proportional to the local absorption coefficient in the sample,[28] in a first approximation, PTIR enables identification of materials[27] and chemical groups[32] by comparison with far-field IR spectral databases. Also, since the PTIR signal derives from the rapid

sample expansion rather than the slower heat diffusion,[33] spatial resolutions as high as ≈ 20 nm[34,35] in contact mode or ≈ 10 nm in tapping-mode[36] are possible. Other recent PTIR innovations include the extension to the visible spectral range[35] and operation in a water environment.[37,38] Due to these characteristics, PTIR impacts an ever-growing number of applications including, polymer science,[39,40] photovoltaics,[41,42] plasmonics,[43,44] geology,[45] biology,[46] and medicine,[47,38,36] as discussed in recent reviews.[26,27] For 2D materials, PTIR has been applied to characterize the polariton distribution in hBN nanostructures[48,49] and to characterize the functional groups in graphene oxide.[50]

In this work, we resonantly excite the AFM cantilever by tuning the laser pulse repetition rate to match one of the cantilever contact-resonance frequencies, thereby amplifying PTIR signal-to-noise ratio by the cantilever's quality (Q) factor, as shown previously.[34] To maintain the cantilever resonant excitation during mapping, a phase-locked loop is used to tie the laser repetition rate to the cantilever oscillation frequency.[36] Using such an excitation scheme, the temperature rise is small (typically less than 1 K)[34] and the thin (< 100 nm) samples analyzed here thermalize back to room temperature between pulses.[31]

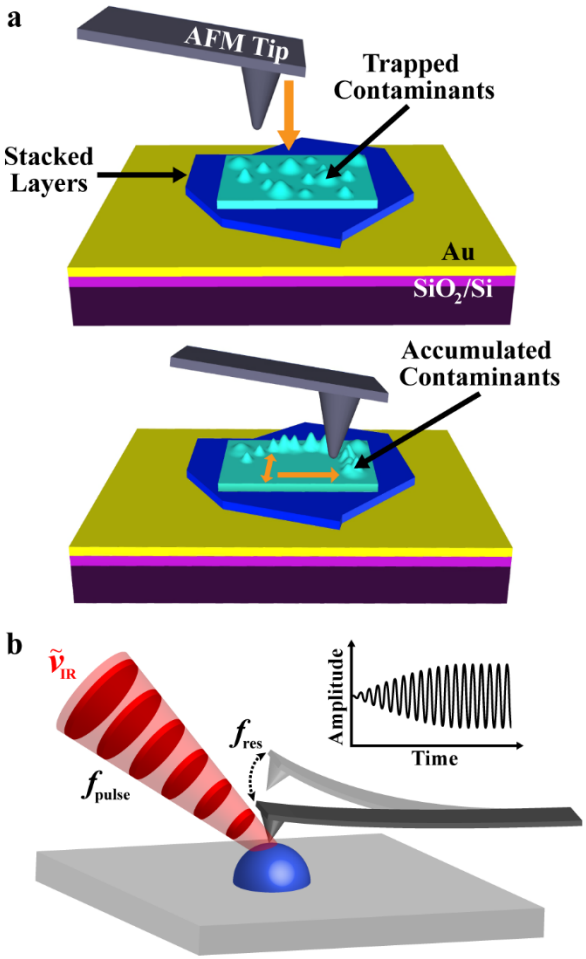

Figure 1. Photothermal induced resonance (PTIR) and nano-squeegee techniques identify the chemical composition of nanoscale contaminants. (a) Schematic illustrating the nano-squeegee technique, which uses the tip of an atomic force microscope probe to sweep trapped contaminants to the periphery of the scanned region. (b) Schematic illustrating PTIR measurements. When infrared (IR) laser pulses are absorbed by the sample, the sample heats up and expands, thereby kicking the cantilever into oscillation. The laser pulse repetition rate (f_{pulse}) is tuned to match one of the cantilever contact-resonant frequencies (f_{res}), leading to enhancement of the oscillation amplitude. The wavenumber ($\tilde{\nu}$) of the impinging IR light is varied to obtain sample absorption spectra.

Heterostructures were assembled from combinations of hBN, tungsten diselenide (WSe_2) and tungsten disulfide (WS_2). Assemblies were obtained using one of three common fabrication techniques that rely on polymeric stamps: (1) PDMS all-dry transfer,[51] (2) water-assisted PDMS pick-up and transfer,[51–54] and (3) polymer-assisted dry pick-up and transfer.[55] While the first two methods employed bare PDMS stamps, the third method used PC-coated PDMS stamps to create 2D materials-based vdWHs. These techniques are described in detail in the Supporting Information (Figures S1–S3). In brief, polymeric stamps were used to pick up and then re-deposit sheets of hBN or TMDs onto complementary flakes through both wet and dry surface-contact processes. The resulting vdWHs exhibited numerous rounded topographic protrusions (e.g., see Figure 2), typically a tell-tale sign of contaminants trapped between the stacked layers.[18,24] The contaminant bubble distribution is driven by competing forces: van der Waals interactions drawing adjacent layers together thereby squeezing contaminants into pockets, while the mechanical stress arising from deformations of the 2D layers favors unstrained layers with uniformly distributed contaminants.[56]

After assembly, the vdWHs were subjected to a nano-squeegee flattening process reported previously.[24] This process, which moves contaminants towards the periphery of a scanning probe raster pattern creates both larger, contaminant-filled bubbles and contaminant-free regions (Figure 1a). For our purposes, both effects are advantageous as they provide areas with enriched contaminant concentrations (i.e., easier to detect), and control regions where little-to-no PTIR signal is expected. Additionally, locally modified regions of the sample exist side-by-side with as-prepared regions, enabling spectroscopic and topographic comparison.

First, we characterize vdWHs fabricated using the water-assisted PDMS pick-up and transfer method. Representative PTIR absorption spectra (Figure 2) were obtained within and

around the nano-squeegeed region of the vdWHs by positioning the probe tip either atop or away from trapped contaminants (bubbles), identified by AFM topography maps. The spectra collected on the nanocontaminants within hBN/hBN vdWHs (Figure 2a) showed prominent absorption peaks at around 1034 cm^{-1}, 1098 cm^{-1} (Si–O–Si stretches), and 1264 cm^{-1} (Si–CH_3 asymmetric deformation), characteristic of PDMS.[57,58] An additional broad peak at about 1376 cm^{-1} is related to hBN phonon-polaritons and possibly to the in-plane phonon mode of hBN.[48,49,59] Spectra measured on the contaminants trapped within TMD-based vdWHs constructed with the same fabrication method (Figure 2b–d) showed similarly prominent peaks (1024 cm^{-1}, 1080 cm^{-1}, and about 1262 cm^{-1}), which we assign to PDMS. Small sample-to-sample differences in the peak positions and band shapes are ascribed to differences in the local environments and, consequently, to different intermolecular interactions[60] between the nanocontaminants and the 2D materials sandwiching them. The nanocontaminant PTIR absorption spectra closely resemble the spectra obtained on macroscopic slabs of PDMS measured via attenuated total reflectance Fourier transform IR (ATR-FTIR) spectroscopy (see Figure S5 in the Supporting Information). In contrast, spectra measured at locations without obvious contamination (i.e., away from bubbles or within the nano-squeegeed region) were notably weaker across their entire spectral range. These spectra, emphasized in Figure S8, however, show broad features that can be attributed for the most part to imperfect background compensation. We attribute the broad, weak features at about 1000 cm^{-1} to SiO_2, which is present as a thin layer in the probe tip and the underlying substrate.

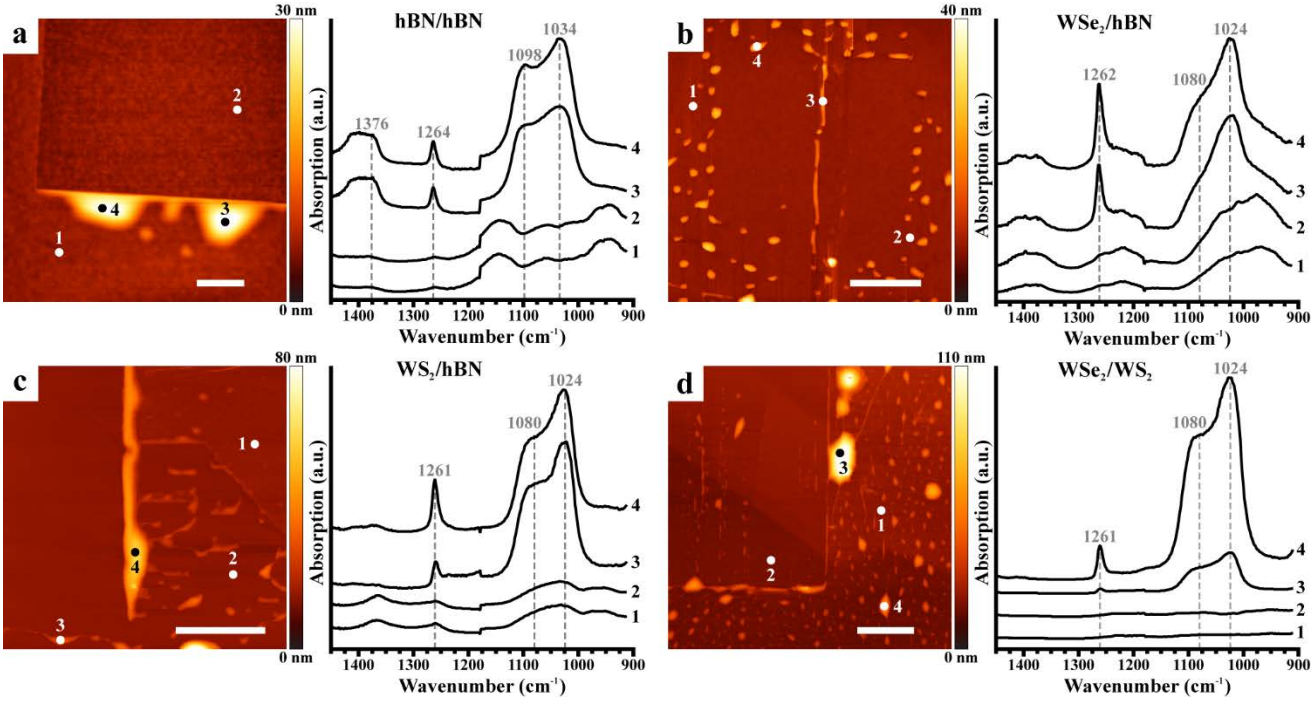

Figure 2. Photothermal induced resonance (PTIR) spectra identify contaminants in van der Waals heterostructures (vdWHs) prepared using the water-assisted PDMS pick-up and transfer method. Representative topographic images (left) and PTIR absorption spectra (right) obtained at the marked locations on vdWHs fabricated by overlaying flakes of (a) hBN/hBN, (b) WSe_2/hBN, (c) WS_2/hBN, and (d) WSe_2/WS_2. Scale bars represent 2 μm.

Next, we analyze representative PTIR absorption spectra obtained on vdWHs fabricated using dry, solvent-free transfer methods (Figure 3). Heterostructures assembled using these methods also exhibited notable topographic features suggestive of trapped contaminants within the stacks of 2D materials. This observation is surprising because the stamps do not touch the contaminated interface during fabrication and no solvent, which might facilitate transport of polymeric residue from the stamp, is used in the process. The spectra of the trapped contaminants within vdWHs assembled using the PDMS all-dry transfer method (Figure 3a) show the strong absorption peaks characteristic of PDMS. We note that the stamps directly contact only the outward facing surfaces of the 2D materials, suggesting the polymer contaminants are itinerant even when using solvent-free methods. In the case of the PDMS stamps, the contamination is attributed to low molecular weight volatile fractions released by the stamp, which adsorb on the exposed surface of the bottom 2D layer and become trapped when depositing the top layer.[61,62] By contrast, spectra measured on vdWHs assembled using PC-coated stamps (Figure 3b) exhibited very different absorption bands. Among the many features evident in these spectra, the prominent peaks at about 1016 cm^{-1}, 1368 cm^{-1}, and 1506 cm^{-1}, are characteristic of O–C–O symmetric deformation, CH_3 symmetric deformation, and aromatic C=C stretch vibrations, respectively.[63,64] These absorption spectra (Figure 3b) show remarkable similarities with ATR-FTIR (Figure S5) and PTIR (Figure S6) spectra measured on PC reference thin films and, notably, lack the characteristic PDMS absorption peaks observed in Figures 2 and 3a. These observations suggest that the contaminants derive only from the exposed stamp surface (PC in this case). Prominent PC absorption peaks were measured both on and away from contaminant bubbles, including inside the nano-squeegeed region and the exposed underlying hBN layer. However, these peaks were absent in spectra measured far (> 1 mm) from the stamp-contacted regions around the vdWHs. As such,

for the PC-coated stamps, the contamination likely is promoted by the higher temperatures used in the fabrication process and incomplete removal of PC by solvents after stacking.[65]

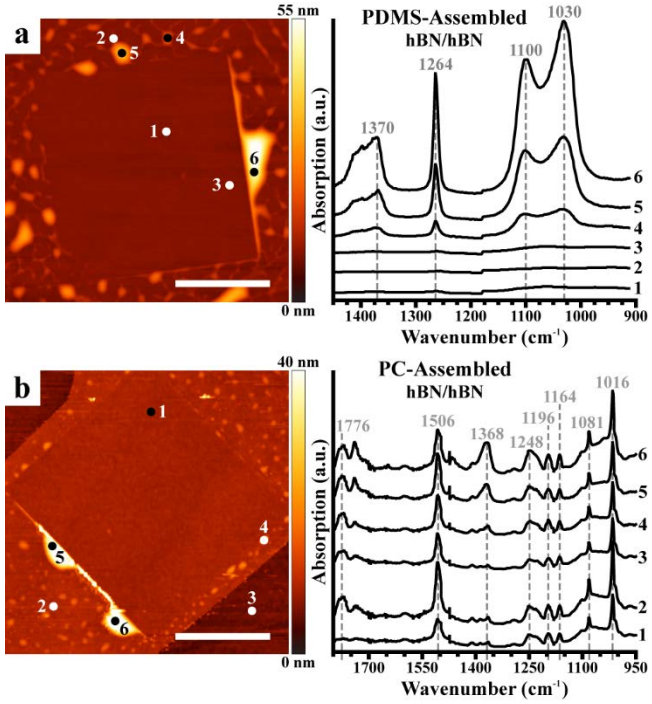

Figure 3. Photothermal induced resonance (PTIR) spectra identify contaminants in van der Waals heterostructures (vdWHs) prepared using 'dry' transfer methods. Topography (left) and PTIR spectra (right) obtained at the marked locations on vdWHs assembled by overlapping flakes of hexagonal boron nitride (hBN/hBN) using the (a) PDMS all-dry transfer method and (b) polymer-assisted dry pick-up and transfer method, which employs stamps coated in polycarbonate (PC). Scale bars represent 5 μm.

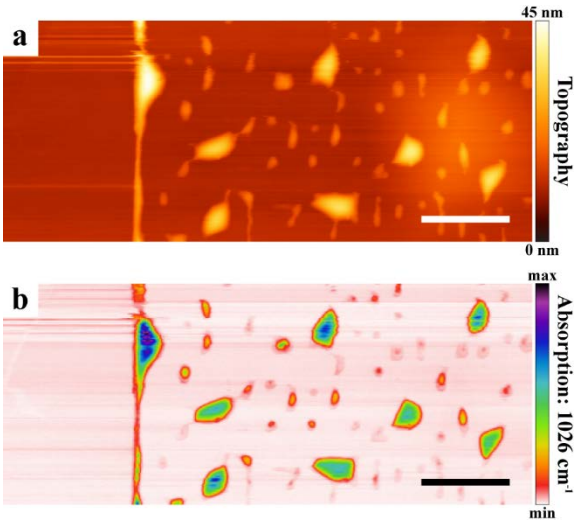

Figure 4. Photothermal induced resonance (PTIR) absorption imaging reveals the nanocontaminant distribution within van der Waals heterostructures (vdWHs). Simultaneously measured (a) topography and (b) PTIR relative absorption maps (Si–O–Si stretch of PDMS, 1026 cm^{-1}) obtained on vdWHs consisting of WSe_2/hBN flakes assembled using the water-assisted PDMS pick-up and transfer method. Scale bars represent 1 µm.

Absorption maps were obtained on vdWHs to assess the relative abundance of contaminants within the scanned region by monitoring absorption at a set wavelength. Figure 4 shows that a PTIR absorption map at 1026 cm^{-1} (Si–O–Si stretch of PDMS) corresponds well to the simultaneously measured topography of a WSe_2/hBN vdWH, prepared using the water-assisted PDMS transfer method, indicating that most contaminant bubbles contain PDMS. These observations clearly suggest that the contaminants consist of PDMS derived from the stamps used in vdWH fabrication. We can also conclude that the regions surrounding the bubbles are largely pristine and free from contaminants. Determining the volumes of contaminant bubbles from the AFM topography maps (Figure S12), and assuming each is filled entirely with PDMS with bulk density of 13 $mol \cdot L^{-1}$,[66] we estimate that some of the smaller bubbles contain as few as ≈ 1.8 amol

of PDMS (see Supporting Information for details). Due to the convolution of the AFM probe tip and contaminant bubble geometries, these measurements overestimate the true bubble sizes and, as such, the amount of material detected shall be considered an upper bound.

Based on these findings, to reduce the stamp-derived contaminants, we devise a stamp cleaning procedure aimed at removing unpolymerized material or other soluble residue from PDMS stamps, prior to vdWH assembly. The PDMS stamps were cleaned with one of four solvents: isopropanol, acetone, toluene, and hexane, and then dried before use. As seen in Figures 5 and S7, vdWHs made using cleaned PDMS stamps (dry transfer) still possess topographic features characteristic of trapped contaminants, with the nano-squeegee process promoting closer contact between the hBN flakes while creating bubbles and a small step around the periphery of the scanned region, which sometimes appears topographically lower than the surrounding region. Without thermal annealing (not used in this work), the top-most 2D layer likely floats on a thin, uniform layer of material, usually < 2 nm thick, separating it from the underlying 2D layer as discussed previously.[24] However, for the structures prepared using stamps cleaned with isopropanol (Figure 5a) and toluene (Figure 5b), the spectra obtained from these bubbles do not show any evidence of PDMS. Instead, broad absorption peaks around 1000 cm^{-1} and 1372 cm^{-1} show that the only detectable signals derive from the SiO_2 and hBN layers. Since the bubble sizes are comparable to those observed in Figures 2–4, but no PDMS or other foreign material is detected, we conclude that either the bubbles are empty or are only partially filled with PDMS contamination in amounts below the detection limit. Another possibility is that the bubbles may be filled with contaminant material that do not possess absorbance features in the examined spectral range, as might be expected for inorganic materials. By contrast, the PTIR spectra of vdWHs prepared with stamps cleaned with acetone or hexane (Figure S7) showed the prominent

characteristic PDMS absorption peaks, suggesting that those solvents were ineffective at reducing or preventing contamination. Additional details regarding stamp cleaning and the characterization of vdWHs assembled from stamps cleaned with other solvents are available in the Supporting Information. These experiments suggest that the abundance and identity of contaminants in vdWHs cannot be assessed based on AFM topography alone and that composition-sensitive methods capable of nanoscale resolution should be employed when possible.

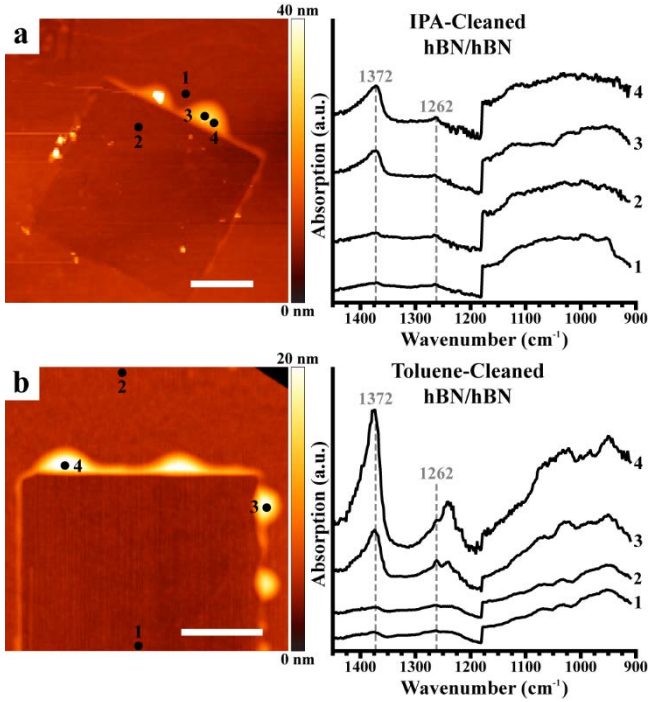

Figure 5. Cleaning polydimethylsiloxane (PDMS) stamps using isopropanol (IPA) and toluene reduces contaminants in van der Waals heterostructures (vdWHs). Topography (left) and photothermal induced resonance absorption spectra (right) obtained at the marked locations on vdWHs fabricated using the all-dry transfer method by overlaying two flakes of hexagonal boron nitride (hBN/hBN) using PDMS stamps pre-cleaned with (a) IPA and (b) toluene. Scale bars represent 2 µm.

CONCLUSIONS

In summary, PTIR absorption spectra and maps enable chemical identification and real space visualization of the nanoscale contaminants commonly found in vdWHs. Clear evidence on vdWHs assembled from 2D materials with different compositions shows that the contaminants consist of residue transferred from the surface of polymeric stamps (PDMS or PC in this work) used in the heterostructure fabrication. Notably, polymer contamination between layers occurs even when 'dry' fabrication methods are used. We found that cleaning PDMS stamps with isopropanol or toluene prior to use reduced the amount of PDMS contaminants trapped within vdWHs. The measurements presented here suggest that the assessment of contaminants in vdWHs should not be conducted based on AFM topographic images alone but, rather, aided by nanoscale composition-sensitive methods, such as PTIR. This analytical approach, coupled with the nano-squeegee procedure, is demonstrated here on vdWHs created with a variety of commonly used fabrication methods, stamps materials, and 2D materials pairs, highlighting its broad applicability to the widespread challenge posed by contaminants trapped between 2D materials, independent from their chemical and mechanical properties. We believe that knowledge of the contaminant composition obtained with the methods presented here will aid better understanding of vdWH properties, which are affected by these impurities, as well as to guide improvements to fabrication techniques to produce intrinsic, contaminant-free heterostructures with precisely tuned properties.

METHODS

PDMS Stamp Preparation. PDMS stamps were prepared using commercially available silicone elastomer kits.[67] The two components (elastomer and curing agent) were mixed in a 10:1 ratio by weight and then degassed under vacuum for 20 min. Next, the mixture was spun onto a

clean, polished silicon wafer and then cured on a hot plate at 80 °C for 30 min. Cured PDMS films (≈ 250 μm thick) were cut into rectangular pieces of varying sizes before use.

PDMS Stamp Cleaning. Only for specific experiments indicated in the manuscript, PDMS stamps were cleaned by immersion in a large excess (> 2000× their volume) of one of four solvents: isopropanol, acetone, toluene, and hexane. The stamps remained immersed for a period of one week while under continuous agitation. Afterward, the stamps were dried for > 24 h in air before use.

Polycarbonate-Coated PDMS Stamp Preparation. A PC polymer solution (6 % mass fraction) was prepared by dissolving solid PC in chloroform. The solution was quickly spread over a SiO_2/Si substrate and the solvent allowed to evaporate, thereby leaving a thin film of PC (≈ 200 nm) coating the surface. These PC/SiO_2/Si substrates were then contacted by PDMS stamps, approximately 1 mm × 2 mm in size. A sharp blade was used to cut the PC films around the periphery of the PDMS stamps. Before removing the stamps, we carefully removed the surrounding PC films using tweezers and then applied drops of deionized water to the edges of the stamps. The water permeated under the PC films, enabling easy removal of PC-coated PDMS stamps. Finally, the PC/PDMS stamps were blown dry with nitrogen gas and placed on glass slides with their PC films exposed (PC/PDMS/glass).

2D Material Deposition. Flakes of hBN were deposited on PDMS, Au-coated SiO_2, and SiO_2 surfaces by mechanical exfoliation from a bulk crystal.[68] Monolayers (and sparingly few bi- and multilayers) of WSe_2 and WS_2 were deposited on SiO_2/Si substrates via chemical vapor deposition.[69] In one case (Figure 2d), an exfoliated flake of WS_2, ≈ 20 nm, was used as the bottom-most layer in a vdWH.

Van der Waals Heterostructure Fabrication. Flakes of various 2D materials (hBN and TMDs) were transferred from their original substrates and stacked to create vdWHs. Flakes were selected with the aid of an optical microscope and manipulated using a custom-built transfer stage. Three transfer processes were used in this study (PDMS All-Dry Transfer, Water-Assisted PDMS Pick-up and Transfer, Polymer-Assisted Dry Pick-up and Transfer), which are described in the Supporting Information.

Nano-squeegee. An AFM-based nano-squeegee[24] procedure was employed to prepare regions of vdWHs with clean, contaminant-free interfaces between stacked 2D materials (see Figure 1a). A relatively dull (or large-diameter) probe tip was used to groom the surface through repeated raster scans, thereby coercing the contaminant bubbles to move to the periphery of the scanned area. The minimum force applied by the probe to induce motion of the trapped contaminants depends on the stiffness (thickness and Young's modulus) of the top, contacted 2D layer. Here, we used the probe in contact mode and first brought the tip to engage on the sample surface while continuously scanning a single line in the area of interest. By gradually increasing the force applied by the tip, the measured topography of the line scan would change; for instance, the apparent heights of the bubbles would decrease with greater tip-surface forces until the feature finally disappeared, indicating tip-induced migration of contaminants. After attaining the requisite force, scanning the area of interest resulted in clearing away the contaminant originally present.

Photothermal Induced Resonance. Gold-coated cantilevers with a nominal spring constant between 0.07–0.4 N/m and nominal first resonance frequency in air of 13 ± 4 kHz were used in the PTIR experiments. The probes were operated in contact mode and the PTIR laser was set to match the third or fourth contact-resonant frequency of the cantilever (≈ 450 kHz or ≈ 700 kHz, respectively). Incident from a quantum cascade laser array with tunable repetition rate

(1 kHz to 2000 kHz) and wavelength (910 cm^{-1} to 1905 cm^{-1}) laser light was polarized parallel to the plane of incidence (p-polarized). Maps of PTIR absorption were obtained using a phase-locked loop with 50–100 kHz bandwidth (centered around the laser repetition rate) to maintain the resonance excitation of the cantilever throughout the image. Absorption spectra were obtained by sweeping the laser wavelength while monitoring the cantilever oscillation amplitude. Absorption maps were obtained by illuminating the sample with a constant wavelength while moving the probe across the sample surface.

ASSOCIATED CONTENT

Supporting Information

The Supporting Information is available free of charge on the ACS Publications website at DOI: 10.1021/acsami.9b06594.

Mass changes of cleaned PDMS stamps, van der Waals heterostructure fabrication methods, molecular structures, spectral and image processing procedures, attenuated total internal reflectance Fourier transform infrared spectra, additional photothermal induced resonance absorption maps, spectra, and topographs, nanocontaminant quantity estimates (PDF)

AUTHOR INFORMATION

Corresponding Authors

*E-mail: berry.jonker@nrl.navy.mil

*E-mail: andrea.centrone@nist.gov

ORCID

Jeffrey J. Schwartz: 0000-0003-1544-1901

Matthew R. Rosenberger: 0000-0001-6866-5488

Kathleen M. McCreary: 0000-0003-2737-585X

Berend T. Jonker: 0000-0001-8816-7857

Andrea Centrone: 0000-0002-2919-3366

Author Contributions

These experiments were designed by J.J.S., H-J.C., and A.C. Heterostructures were fabricated and nano-squeegeed by H-J.C. and M.R.R. S.V.S. and K.M.M. synthesized the monolayer TMD materials. Infrared (ATR-FTIR and PTIR) spectra, absorption maps, and topography images were

measured by J.J.S and analyzed by J.J.S. and A.C. Figures were prepared by J.J.S. and H-J.C. The manuscript was written by J.J.S. with contributions from all authors. All authors have given approval to the final version of the manuscript.

Notes

The authors declare no competing financial interest.

ACKNOWLEDGMENTS

J.J.S. acknowledges support under the Corporative Research Agreement between the University of Maryland and the National Institute of Standards and Technology, Award 70NANB14H209, through the University of Maryland. H.-J.C. acknowledges support from an American Society for Engineering Education fellowship. M.R.R. and S.V.S. acknowledge support from National Research Council fellowships.

REFERENCES

(1) Novoselov, K. S.; Jiang, D.; Schedin, F.; Booth, T. J.; Khotkevich, V. V.; Morozov, S. V.; Geim, A. K. Two-Dimensional Atomic Crystals. *Proc. Natl. Acad. Sci. U.S.A.* **2005**, *102* (30), 10451–10453. https://doi.org/10.1073/pnas.0502848102.

(2) Wang, Q. H.; Kalantar-Zadeh, K.; Kis, A.; Coleman, J. N.; Strano, M. S. Electronics and Optoelectronics of Two-Dimensional Transition Metal Dichalcogenides. *Nat. Nanotechnol.* **2012**, *7* (11), 699–712. https://doi.org/10.1038/nnano.2012.193.

(3) Zhang, K.; Feng, Y.; Wang, F.; Yang, Z.; Wang, J. Two Dimensional Hexagonal Boron Nitride (2D-HBN): Synthesis, Properties and Applications. *J. Mater. Chem. C* **2017**, *5* (46), 11992–12022. https://doi.org/10.1039/C7TC04300G.

(4) Mas-Ballesté, R.; Gómez-Navarro, C.; Gómez-Herrero, J.; Zamora, F. 2D Materials: To Graphene and Beyond. *Nanoscale* **2011**, *3* (1), 20–30. https://doi.org/10.1039/C0NR00323A.

(5) Novoselov, K. S.; Mishchenko, A.; Carvalho, A.; Neto, A. H. C. 2D Materials and van Der Waals Heterostructures. *Science* **2016**, *353* (6298), aac9439. https://doi.org/10.1126/science.aac9439.

(6) Zhang, Y.; Rubio, A.; Lay, G. L. Emergent Elemental Two-Dimensional Materials beyond Graphene. *J. Phys. D: Appl. Phys.* **2017**, *50* (5), 053004. https://doi.org/10.1088/1361-6463/aa4e8b.

(7) Novoselov, K. S.; Neto, A. H. C. Two-Dimensional Crystals-Based Heterostructures: Materials with Tailored Properties. *Phys. Scr.* **2012**, *T146*, 014006. https://doi.org/10.1088/0031-8949/2012/T146/014006.

(8) Liu, Y.; Weiss, N. O.; Duan, X.; Cheng, H.-C.; Huang, Y.; Duan, X. Van Der Waals Heterostructures and Devices. *Nat. Rev. Mater.* **2016**, *1*, 16042. https://doi.org/10.1038/natrevmats.2016.42.

(9) Hamann, D. M.; Hadland, E. C.; Johnson, D. C. Heterostructures Containing Dichalcogenides-New Materials with Predictable Nanoarchitectures and Novel Emergent Properties. *Semicond. Sci. Technol.* **2017**, *32* (9), 093004. https://doi.org/10.1088/1361-6641/aa7785.

(10) Lee, G.-H.; Cui, X.; Kim, Y. D.; Arefe, G.; Zhang, X.; Lee, C.-H.; Ye, F.; Watanabe, K.; Taniguchi, T.; Kim, P.; Hone, J. Highly Stable, Dual-Gated MoS_2 Transistors Encapsulated by Hexagonal Boron Nitride with Gate-Controllable Contact, Resistance, and Threshold Voltage. *ACS Nano* **2015**, *9* (7), 7019–7026. https://doi.org/10.1021/acsnano.5b01341.

(11) Deng, D.; Novoselov, K. S.; Fu, Q.; Zheng, N.; Tian, Z.; Bao, X. Catalysis with Two-Dimensional Materials and Their Heterostructures. *Nat. Nanotechnol.* **2016**, *11* (3), 218–230. https://doi.org/10.1038/nnano.2015.340.

(12) Cao, Y.; Fatemi, V.; Fang, S.; Watanabe, K.; Taniguchi, T.; Kaxiras, E.; Jarillo-Herrero, P. Unconventional Superconductivity in Magic-Angle Graphene Superlattices. *Nature* **2018**, *556* (7699), 43–50. https://doi.org/10.1038/nature26160.

(13) Dean, C. R.; Young, A. F.; Meric, I.; Lee, C.; Wang, L.; Sorgenfrei, S.; Watanabe, K.; Taniguchi, T.; Kim, P.; Shepard, K. L.; Hone, J. Boron Nitride Substrates for High-Quality Graphene Electronics. *Nat. Nanotechnol.* **2010**, *5* (10), 722–726. https://doi.org/10.1038/nnano.2010.172.

(14) Schneider, G. F.; Calado, V. E.; Zandbergen, H.; Vandersypen, L. M. K.; Dekker, C. Wedging Transfer of Nanostructures. *Nano Lett.* **2010**, *10* (5), 1912–1916. https://doi.org/10.1021/nl1008037.

(15) Castellanos-Gomez, A.; Buscema, M.; Molenaar, R.; Singh, V.; Janssen, L.; Zant, H. S. J. van der; Steele, G. A. Deterministic Transfer of Two-Dimensional Materials by All-Dry Viscoelastic Stamping. *2D Mater.* **2014**, *1* (1), 011002. https://doi.org/10.1088/2053-1583/1/1/011002.

(16) Wang, L.; Meric, I.; Huang, P. Y.; Gao, Q.; Gao, Y.; Tran, H.; Taniguchi, T.; Watanabe, K.; Campos, L. M.; Muller, D. A.; Guo, J.; Kim, P.; Hone, J.; Shepard, K. L.; Dean, C. R. One-Dimensional Electrical Contact to a Two-Dimensional Material. *Science* **2013**, *342* (6158), 614–617. https://doi.org/10.1126/science.1244358.

(17) Pizzocchero, F.; Gammelgaard, L.; Jessen, B. S.; Caridad, J. M.; Wang, L.; Hone, J.; Bøggild, P.; Booth, T. J. The Hot Pick-up Technique for Batch Assembly of van Der Waals Heterostructures. *Nat. Commun.* **2016**, *7*, 11894. https://doi.org/10.1038/ncomms11894.

(18) Haigh, S. J.; Gholinia, A.; Jalil, R.; Romani, S.; Britnell, L.; Elias, D. C.; Novoselov, K. S.; Ponomarenko, L. A.; Geim, A. K.; Gorbachev, R. Cross-Sectional Imaging of Individual Layers and Buried Interfaces of Graphene-Based Heterostructures and Superlattices. *Nat. Mater.* **2012**, *11* (9), 764–767. https://doi.org/10.1038/nmat3386.

(19) Alexeev, E. M.; Catanzaro, A.; Skrypka, O. V.; Nayak, P. K.; Ahn, S.; Pak, S.; Lee, J.; Sohn, J. I.; Novoselov, K. S.; Shin, H. S.; Tartakovskii, A. I. Imaging of Interlayer Coupling in van Der Waals Heterostructures Using a Bright-Field Optical Microscope. *Nano Lett.* **2017**, *17* (9), 5342–5349. https://doi.org/10.1021/acs.nanolett.7b01763.

(20) Kuriakose, S.; Ahmed, T.; Balendhran, S.; Bansal, V.; Sriram, S.; Bhaskaran, M.; Walia, S. Black Phosphorus: Ambient Degradation and Strategies for Protection. *2D Mater.* **2018**, *5* (3), 032001. https://doi.org/10.1088/2053-1583/aab810.

(21) Huang, Y.; Qiao, J.; He, K.; Bliznakov, S.; Sutter, E.; Chen, X.; Luo, D.; Meng, F.; Su, D.; Decker, J.; Ji, W.; Ruoff, R. S.; Sutter, P. Interaction of Black Phosphorus with Oxygen and Water. *Chem. Mater.* **2016**, *28* (22), 8330–8339. https://doi.org/10.1021/acs.chemmater.6b03592.

(22) Purdie, D. G.; Pugno, N. M.; Taniguchi, T.; Watanabe, K.; Ferrari, A. C.; Lombardo, A. Cleaning Interfaces in Layered Materials Heterostructures. *Nat. Commun.* **2018**, *9* (1), 5387. https://doi.org/10.1038/s41467-018-07558-3.

(23) Lindvall, N.; Kalabukhov, A.; Yurgens, A. Cleaning Graphene Using Atomic Force Microscope. *J. Appl. Phys.* **2012**, *111* (6), 064904. https://doi.org/10.1063/1.3695451.

(24) Rosenberger, M. R.; Chuang, H.-J.; McCreary, K. M.; Hanbicki, A. T.; Sivaram, S. V.; Jonker, B. T. Nano-"Squeegee" for the Creation of Clean 2D Material Interfaces. *ACS Appl. Mater. Interfaces* **2018**, *10* (12), 10379–10387. https://doi.org/10.1021/acsami.8b01224.

(25) Kang, K.; Lee, K.-H.; Han, Y.; Gao, H.; Xie, S.; Muller, D. A.; Park, J. Layer-by-Layer Assembly of Two-Dimensional Materials into Wafer-Scale Heterostructures. *Nature* **2017**, *550* (7675), 229–233. https://doi.org/10.1038/nature23905.

(26) Centrone, A. Infrared Imaging and Spectroscopy Beyond the Diffraction Limit. *Annu. Rev. Anal. Chem.* **2015**, *8* (1), 101–126. https://doi.org/10.1146/annurev-anchem-071114-040435.

(27) Dazzi, A.; Prater, C. B. AFM-IR: Technology and Applications in Nanoscale Infrared Spectroscopy and Chemical Imaging. *Chem. Rev.* **2017**, *117* (7), 5146–5173. https://doi.org/10.1021/acs.chemrev.6b00448.

(28) Dazzi, A.; Glotin, F.; Carminati, R. Theory of Infrared Nanospectroscopy by Photothermal Induced Resonance. *J. Appl. Phys.* **2010**, *107* (12), 124519. https://doi.org/10.1063/1.3429214.

(29) Lahiri, B.; Holland, G.; Centrone, A. Chemical Imaging Beyond the Diffraction Limit: Experimental Validation of the PTIR Technique. *Small* **2013**, *9* (3), 439–445. https://doi.org/10.1002/smll.201200788.

(30) Ramer, G.; Aksyuk, V. A.; Centrone, A. Quantitative Chemical Analysis at the Nanoscale Using the Photothermal Induced Resonance Technique. *Anal. Chem.* **2017**, *89* (24), 13524–13531. https://doi.org/10.1021/acs.analchem.7b03878.

(31) Chae, J.; An, S.; Ramer, G.; Stavila, V.; Holland, G.; Yoon, Y.; Talin, A. A.; Allendorf, M.; Aksyuk, V. A.; Centrone, A. Nanophotonic Atomic Force Microscope Transducers Enable Chemical Composition and Thermal Conductivity Measurements at the Nanoscale. *Nano Lett.* **2017**, *17* (9), 5587–5594. https://doi.org/10.1021/acs.nanolett.7b02404.

(32) Katzenmeyer, A. M.; Canivet, J.; Holland, G.; Farrusseng, D.; Centrone, A. Assessing Chemical Heterogeneity at the Nanoscale in Mixed-Ligand Metal–Organic Frameworks with the PTIR Technique. *Angew. Chem., Int. Ed.*. **2014**, *53* (11), 2852–2856. https://doi.org/10.1002/anie.201309295.

(33) Katzenmeyer, A. M.; Holland, G.; Chae, J.; Band, A.; Kjoller, K.; Centrone, A. Mid-Infrared Spectroscopy beyond the Diffraction Limit via Direct Measurement of the

Photothermal Effect. *Nanoscale* **2015**, *7* (42), 17637–17641. https://doi.org/10.1039/C5NR04854K.

(34) Lu, F.; Jin, M.; Belkin, M. A. Tip-Enhanced Infrared Nanospectroscopy via Molecular Expansion Force Detection. *Nat. Photonics* **2014**, *8* (4), 307–312. https://doi.org/10.1038/nphoton.2013.373.

(35) Katzenmeyer, A. M.; Holland, G.; Kjoller, K.; Centrone, A. Absorption Spectroscopy and Imaging from the Visible through Mid-Infrared with 20 nm Resolution. *Anal. Chem.* **2015**, *87* (6), 3154–3159. https://doi.org/10.1021/ac504672t.

(36) Wieland, K.; Ramer, G.; Weiss, V. U.; Allmaier, G.; Lendl, B.; Centrone, A. Nanoscale Chemical Imaging of Individual Chemotherapeutic Cytarabine-Loaded Liposomal Nanocarriers. *Nano Res.* **2019**, *12* (1), 197–203. https://doi.org/10.1007/s12274-018-2202-x.

(37) Jin, M.; Lu, F.; Belkin, M. A. High-Sensitivity Infrared Vibrational Nanospectroscopy in Water. *Light Sci. Appl.* **2017**, *6* (7), e17096. https://doi.org/10.1038/lsa.2017.96.

(38) Ramer, G.; Ruggeri, F. S.; Levin, A.; Knowles, T. P. J.; Centrone, A. Determination of Polypeptide Conformation with Nanoscale Resolution in Water. *ACS Nano* **2018**, *12* (7), 6612–6619. https://doi.org/10.1021/acsnano.8b01425.

(39) Morsch, S.; Liu, Y.; Lyon, S. B.; Gibbon, S. R. Insights into Epoxy Network Nanostructural Heterogeneity Using AFM-IR. *ACS Appl. Mater. Interfaces* **2016**, *8* (1), 959–966. https://doi.org/10.1021/acsami.5b10767.

(40) Tri, P. N.; Prud'homme, R. E. Nanoscale Lamellar Assembly and Segregation Mechanism of Poly(3-Hydroxybutyrate)/Poly(Ethylene Glycol) Blends. *Macromolecules* **2018**, *51* (1), 181–188. https://doi.org/10.1021/acs.macromol.7b02019.

(41) Strelcov, E.; Dong, Q.; Li, T.; Chae, J.; Shao, Y.; Deng, Y.; Gruverman, A.; Huang, J.; Centrone, A. $CH_3NH_3PbI_3$ Perovskites: Ferroelasticity Revealed. *Sci. Adv.* **2017**, *3* (4), e1602165. https://doi.org/10.1126/sciadv.1602165.

(42) Chae, J.; Dong, Q.; Huang, J.; Centrone, A. Chloride Incorporation Process in $CH_3NH_3PbI_{3-x}Cl_x$ Perovskites via Nanoscale Bandgap Maps. *Nano Lett.* **2015**, *15* (12), 8114–8121. https://doi.org/10.1021/acs.nanolett.5b03556.

(43) Katzenmeyer, A. M.; Chae, J.; Kasica, R.; Holland, G.; Lahiri, B.; Centrone, A. Nanoscale Imaging and Spectroscopy of Plasmonic Modes with the PTIR Technique. *Adv. Opt. Mater.* **2014**, *2* (8), 718–722. https://doi.org/10.1002/adom.201400005.

(44) Mancini, A.; Giliberti, V.; Alabastri, A.; Calandrini, E.; De Angelis, F.; Garoli, D.; Ortolani, M. Thermoplasmonic Effect of Surface-Enhanced Infrared Absorption in Vertical Nanoantenna Arrays. *J. Phys. Chem. C* **2018**, *122* (24), 13072–13081. https://doi.org/10.1021/acs.jpcc.8b03808.

(45) Kebukawa, Y.; Kobayashi, H.; Urayama, N.; Baden, N.; Kondo, M.; Zolensky, M. E.; Kobayashi, K. Nanoscale Infrared Imaging Analysis of Carbonaceous Chondrites to Understand Organic-Mineral Interactions during Aqueous Alteration. *Proc. Natl. Acad. Sci. U.S.A.* **2019**, *116* (3), 753–758. https://doi.org/10.1073/pnas.1816265116.

(46) Dazzi, A.; Prater, C. B.; Hu, Q.; Chase, D. B.; Rabolt, J. F.; Marcott, C. AFM–IR: Combining Atomic Force Microscopy and Infrared Spectroscopy for Nanoscale Chemical Characterization. *Appl. Spectrosc.* **2012**, *66* (12), 1365–1384. https://doi.org/10.1366/12-06804.

(47) Ruggeri, F. S.; Longo, G.; Faggiano, S.; Lipiec, E.; Pastore, A.; Dietler, G. Infrared Nanospectroscopy Characterization of Oligomeric and Fibrillar Aggregates during Amyloid Formation. *Nat. Commun.* **2015**, *6*, 7831. https://doi.org/10.1038/ncomms8831.

(48) Brown, L. V.; Davanco, M.; Sun, Z.; Kretinin, A.; Chen, Y.; Matson, J. R.; Vurgaftman, I.; Sharac, N.; Giles, A. J.; Fogler, M. M.; Taniguchi, T.; Watanabe, K.; Novoselov, K. S.; Maier, S. A.; Centrone, A.; Caldwell, J. D. Nanoscale Mapping and Spectroscopy of Nonradiative Hyperbolic Modes in Hexagonal Boron Nitride Nanostructures. *Nano Lett.* **2018**, *18* (3), 1628–1636. https://doi.org/10.1021/acs.nanolett.7b04476.

(49) Ciano, C.; Giliberti, V.; Ortolani, M.; Baldassarre, L. Observation of Phonon-Polaritons in Thin Flakes of Hexagonal Boron Nitride on Gold. *Appl. Phys. Lett.* **2018**, *112* (15), 153101. https://doi.org/10.1063/1.5024518.

(50) Liu, Z.; Nørgaard, K.; Overgaard, M. H.; Ceccato, M.; Mackenzie, D. M. A.; Stenger, N.; Stipp, S. L. S.; Hassenkam, T. Direct Observation of Oxygen Configuration on Individual Graphene Oxide Sheets. *Carbon* **2018**, *127*, 141–148. https://doi.org/10.1016/j.carbon.2017.10.100.

(51) Chuang, H.-J.; Chamlagain, B.; Koehler, M.; Perera, M. M.; Yan, J.; Mandrus, D.; Tománek, D.; Zhou, Z. Low-Resistance 2D/2D Ohmic Contacts: A Universal Approach to High-Performance WSe_2, MoS_2, and $MoSe_2$ Transistors. *Nano Lett.* **2016**, *16* (3), 1896–1902. https://doi.org/10.1021/acs.nanolett.5b05066.

(52) Xu, M.; Liang, T.; Shi, M.; Chen, H. Graphene-Like Two-Dimensional Materials. *Chem. Rev.* **2013**, *113* (5), 3766–3798. https://doi.org/10.1021/cr300263a.

(53) Hanbicki, A. T.; Chuang, H.-J.; Rosenberger, M. R.; Hellberg, C. S.; Sivaram, S. V.; McCreary, K. M.; Mazin, I. I.; Jonker, B. T. Double Indirect Interlayer Exciton in a

$MoSe_2/WSe_2$ van Der Waals Heterostructure. *ACS Nano* **2018**, *12* (5), 4719–4726. https://doi.org/10.1021/acsnano.8b01369.

(54) Jia, H.; Yang, R.; Nguyen, A. E.; Alvillar, S. N.; Empante, T.; Bartels, L.; Feng, P. X.-L. Large-Scale Arrays of Single- and Few-Layer MoS_2 Nanomechanical Resonators. *Nanoscale* **2016**, *8* (20), 10677–10685. https://doi.org/10.1039/C6NR01118G.

(55) Zomer, P. J.; Guimarães, M. H. D.; Brant, J. C.; Tombros, N.; van Wees, B. J. Fast Pick up Technique for High Quality Heterostructures of Bilayer Graphene and Hexagonal Boron Nitride. *Appl. Phys. Lett.* **2014**, *105* (1), 013101. https://doi.org/10.1063/1.4886096.

(56) Khestanova, E.; Guinea, F.; Fumagalli, L.; Geim, A. K.; Grigorieva, I. V. Universal Shape and Pressure inside Bubbles Appearing in van Der Waals Heterostructures. *Nat. Commun.* **2016**, *7*, 12587. https://doi.org/10.1038/ncomms12587.

(57) Groza, A.; Surmeian, A. Characterization of the Oxides Present in a Polydimethylsiloxane Layer Obtained by Polymerisation of Its Liquid Precursor in Corona Discharge. *J. Nanomater.* **2015**, *2015*, 1–8. http://dx.doi.org/10.1155/2015/204296.

(58) Lin-Vien, D.; Colthup, N. B.; Fateley, W. G.; Grasselli, J. G. Organosilicon Compounds. In *The Handbook of Infrared and Raman Characteristic Frequencies of Organic Molecules*; Lin-Vien, D., Colthup, N. B., Fateley, W. G., Grasselli, J. G., Eds.; Academic Press: San Diego, 1991; pp 251–261. https://doi.org/10.1016/B978-0-08-057116-4.50021-3.

(59) Geick, R.; Perry, C. H.; Rupprecht, G. Normal Modes in Hexagonal Boron Nitride. *Phys. Rev.* **1966**, *146* (2), 543–547. https://doi.org/10.1103/PhysRev.146.543.

(60) Centrone, A.; Brambilla, L.; Zerbi, G. Adsorption of H_2 on Carbon-Based Materials: A Raman Spectroscopy Study. *Phys. Rev. B* **2005**, *71* (24), 245406. https://doi.org/10.1103/PhysRevB.71.245406.

(61) Andersson, L. H. U.; Hjertberg, T. Silicone Elastomers for Electronic Applications. I. Analyses of the Noncrosslinked Fractions. *J. Appl. Polym. Sci.* **2003**, *88* (8), 2073–2081. https://doi.org/10.1002/app.12027.

(62) Glasmästar, K.; Gold, J.; Andersson, A.-S.; Sutherland, D. S.; Kasemo, B. Silicone Transfer during Microcontact Printing. *Langmuir* **2003**, *19* (13), 5475–5483. https://doi.org/10.1021/la026558x.

(63) Schnell, H. *Chemistry and Physics of Polycarbonates*; Interscience Publishers: New York, 1964; Vol. 9.

(64) Silverstein, R. M.; Webster, F. X.; Kiemle, D. *Spectrometric Identification of Organic Compounds, 7th Edition*; Wiley, 2005.

(65) Lin, Y.-C.; Lu, C.-C.; Yeh, C.-H.; Jin, C.; Suenaga, K.; Chiu, P.-W. Graphene Annealing: How Clean Can It Be? *Nano Lett.* **2012**, *12* (1), 414–419. https://doi.org/10.1021/nl203733r.

(66) Chemical Retrieval on the Web. Poly(dimethylsiloxane) https://polymerdatabase.com/polymers/Polydimethylsiloxane.html (accessed Mar 1, 2019).

(67) Lee, J. N.; Park, C.; Whitesides, G. M. Solvent Compatibility of Poly(Dimethylsiloxane)-Based Microfluidic Devices. *Anal. Chem.* **2003**, *75* (23), 6544–6554. https://doi.org/10.1021/ac0346712.

(68) Wang, Z.; Tang, Z.; Xue, Q.; Huang, Y.; Huang, Y.; Zhu, M.; Pei, Z.; Li, H.; Jiang, H.; Fu, C.; Zhi, C. Fabrication of Boron Nitride Nanosheets by Exfoliation. *Chem. Rec.* **2016**, *16* (3), 1204–1215. https://doi.org/10.1002/tcr.201500302.

(69) McCreary, K. M.; Hanbicki, A. T.; Jernigan, G. G.; Culbertson, J. C.; Jonker, B. T. Synthesis of Large-Area WS_2 Monolayers with Exceptional Photoluminescence. *Sci. Rep.* **2016**, *6*, 19159. https://doi.org/10.1038/srep19159.

For Table of Contents Only